



1

2

3 **Mapping global forest age from forest inventories, biomass and climate data**

4 Simon Besnard^{1,2}, Sujan Koirala¹, Maurizio Santoro⁵, Ulrich Weber¹, Jacob Nelson¹, Jonas Gütter^{1,4},
5 Bruno Herault^{6,7}, Justin Kassi⁸, Anny N'Guessan⁸, Christopher Neigh⁹, Benjamin Poulter⁹, Tao
6 Zhang^{10,11}, Nuno Carvalhais^{1,3}

7

8 ¹Max Planck Institute for Biogeochemistry, Germany

9 ²Laboratory of Geo-Information Science and Remote Sensing, Wageningen University & Research, The Netherlands

10 ³Departamento de Ciências e Engenharia do Ambiente, DCEA, Faculdade de Ciências e Tecnologia, FCT, Universidade
11 Nova de Lisboa, Portugal

12 ⁴DLR, Institute of Data Science Data Management and Analysis, Germany

13 ⁵Gamma Remote Sensing, Switzerland

14 ⁶INP-HB, Institut National Polytechnique Félix Houphouët-Boigny, Côte d'Ivoire

15 ⁷Cirad, University of Montpellier, UR Forests & Societies, France

16 ⁸Université Félix Houphouët-Boigny, UFR Biosciences, Laboratoire de Botanique, Côte d'Ivoire

17 ⁹NASA Goddard Space Flight Center, Biospheric Sciences Lab., Greenbelt, MD, USA

18 ¹⁰University of Florida, Department of Biology, United States

19 ¹¹University of Minnesota, Department of Forest Resources, United States

20

21 *Correspondence to:* Simon Besnard (sbesnard@bgc-jena.mpg.de) and Nuno Carvalhais (ncarvalhais@bgc-jena.mpg.de)



22 **Abstract.** Forest age can determine the capacity of a forest to uptake carbon from the atmosphere. Yet, a lack of global
23 diagnostics that reflect the forest stage and associated disturbance regimes hampers the quantification of age-related
24 differences in forest carbon dynamics. In this study, we provide a new global distribution of forest age circa 2010,
25 estimated using a machine learning approach trained with more than 40,000 plots using forest inventory, biomass and
26 climate data. First, evaluation against the plot level forest age measurements reveals that the data-driven method has a
27 relatively good predictive capacity of classifying old-growth vs. non-old-growth (precision = 0.81 and 0.99 for old-
28 growth and non-old-growth, respectively) forests and estimating corresponding forest ages (NSE = 0.6 and RMSE = 50
29 years). Yet, there are systematic biases with overestimation in young and underestimation in old forest stands,
30 respectively. Globally, we find a large variability of forest age with the old-growth forests in the tropical regions of
31 Amazon and Congo, and young forests in China and intermediate stands in Europe. On the other hand, we find that the
32 regions with high rates of deforestation or forest degradation (e.g., the arc of deforestation in the Amazon) are largely
33 composed of younger stands. Assessment of forest age in the climate-space shows that the old-forests are either in cold
34 and dry regions or in warm and wet regions, while young-intermediate forests span a large climatic gradient. Finally, a
35 comparison between the presented forest age estimates with a series of regional products reveals differences rooted in
36 different approaches as well as in different in-situ observations and global-scale products. Despite showing robustness
37 in cross-validation results, additional methodological insights on further developments should as much as possible
38 harmonize data across the different approaches. The forest age dataset presented here provides additional insights into
39 the global distribution of forest age in support of a better understanding of the global dynamics in the forest water and
40 carbon cycles. The forest age datasets are openly available at <https://doi.org/10.17871/ForestAgeBGI.2021> (Besnard et
41 al., 2021). For anonymous access during review, please refer to the data availability section below.

42 1 Introduction

43 Forests cover about 30% of the terrestrial surface of our planet and store a large part of the terrestrial carbon, indicating
44 their fundamental role in the terrestrial carbon cycle (Bar-On, Phillips, and Milo, 2018). Yet, drivers controlling the
45 capacity of the terrestrial biosphere to sequester carbon remain poorly characterized, limiting our understanding of the
46 global land carbon sink's location (Cook-Patton et al., 2020). Such uncertainties on the geographical distribution of the
47 carbon sink have been partly attributed to the fact that forest regrowth and demography are not systematically
48 considered for understanding changes in the forest carbon sink (Pugh et al., 2019, Zscheischler et al., 2017).

49 While the recent increase in the forest carbon sink is controlled by environmental changes such as carbon dioxide (CO₂)
50 fertilization, nitrogen deposition, and climate change (Zhu et al., 2016), the dynamics in the forest carbon balance are
51 also attributed to disturbance history and forest regrowth (Pugh et al., 2019; Besnard et al. 2019; Amiro et al., 2010).
52 Forest disturbances cause physical damages to vegetation properties and changes in forest demography, thereby
53 affecting the balance of terrestrial CO₂ exchange with the atmosphere by temporarily increasing respiration and
54 reducing photosynthesis (Birdsey et al., 2006; Johnson and Curtis, 2001; Liu et al., 2011; Schimel, 2007; Williams et
55 al., 2012; Woodbury et al., 2007). The changes in the strength of carbon uptake or release can alter the forest carbon
56 balance by converting forest ecosystems from carbon sinks to sources (Amiro et al., 2010; Bowman et al., 2009; Ciais et
57 al., 2014; Moore et al., 2013). Odum (1969) hypothesized the first theory to describe the ecosystem development in the
58 absence of major disturbance, suggesting that the age of forests and how demographic changes drive carbon
59 accumulation. Yet, an intrinsic property of a stand can be modified to varying degrees of changes in environmental



60 conditions and disturbance, therefore slowly change along with a forest age or successional continuum (Irvine et al.,
61 2005; Piponiot et al., 2018).

62 Despite the sensitivity of the forest carbon balance to disturbance and regrowth (Buitenwerf et al., 2018; Sulla-Menashe
63 et al., 2018), existing empirical models and current bottom-up spatiotemporal assessment of CO₂ fluxes do not
64 explicitly account for these effects (Jung et al., 2020; Tramontana et al., 2016; Jung et al., 2011). By not explicitly
65 constraining data-driven statistical models with disturbance history or forest demography, the forest carbon balance in
66 regions with newly disturbed forests and old-growth forests may not be realistically estimated. For instance, large
67 discrepancies are observed between statistical bottom-up approaches (e.g., FLUXCOM initiatives,
68 <http://www.fluxcom.org/>) and atmospheric inversions in estimating net ecosystem exchange (NEE), particularly in the
69 tropics where site history plays a substantial role in NEE magnitude (Pugh et al., 2019). To account for the contribution
70 of disturbance on the land carbon sink, information on the geographical distribution of disturbance is therefore required,
71 albeit such information is rather limited at the global scale (Ciais et al., 2014). Forest age, related to time since
72 disturbance, can be seen as a useful surrogate in analyses of the impact of disturbance on the ability of forests to
73 sequester and store carbon. Incorporating forest age into terrestrial biosphere modelling offers a starting point to
74 characterize disturbance history, therefore to get more insights on the location of the terrestrial carbon sinks (Pugh et al.,
75 2019). Reliable estimates of gridded forest age are, therefore, an important and needed source of information. The
76 recent advances in describing the geographical distribution of forest demography globally (Huang et al., 2010; Kennedy
77 et al., 2010; Poulter et al., 2019) have paved the way to consider forest age and disturbance history in carbon cycle
78 studies.

79 Here, we aim to provide a new gridded global forest age dataset *circa* 2010 inferred from a compilation of forest
80 inventory, biomass and climate data. More specifically, we introduce the *in-situ* forest inventory dataset and the
81 modelling framework used in this study as well as the predictive capacity of the presented model to infer forest age at
82 the plot level. We further describe the global and regional patterns of the gridded forest age dataset and their
83 uncertainties. The presented forest age dataset is finally benchmarked against a series of independent regional and
84 global datasets.

85 **2 Method**

86 **2.1 Forest inventory and climate data**

87 The globally gridded forest age dataset was developed by collecting *in-situ* plot level stand age, and aboveground
88 biomass (AGB) estimates from a series of forest inventory databases (Álvarez-Dávila et al., 2017; Anderson-Teixeira et
89 al., 2018; Anderson-Teixeira et al., 2016; Baker et al., 2016; Johnson et al., 2016; Lewis et al., 2013; Mitchard et al.,
90 2014; N'Guessan et al., 2019; Poorter et al., 2016; Schepaschenko et al., 2017; Somogyi et al., 2008; Sullivan et al.,
91 2017). Besides, we sampled 20,000 observations from the US Forest Service Forest Inventory and Analysis (FIA) data
92 (Burill et al. 2018) containing *in-situ* plot level stand age and aboveground biomass (AGB) estimates (the original
93 number of observations in the FIA dataset = 350,000). To reduce the unbalanced sample size across age classes, we
94 weight-sampled the FIA data with decadal age classes that are underrepresented in the dataset before including the FIA
95 data having higher weights. The weights for each decadal class were calculated following Eq. (1):

$$96 \text{weight}_i = \frac{\sum_{i=1}^n N \text{age class}_i}{\text{Total } N} \quad (1)$$



97 Where i is a decadal class and N is the number of observations.

98 The methods used in inventory surveys to estimate stand age relied on expert knowledge, tree diameter measurements,
99 tree rings from cores of selected trees (e.g., Burill et al. 2018), and/or semi-directive interviews (e.g., N'Guessan et al.,
100 2019). Forest inventory plots were classified as old-growth forests when stand age was more than or equal to 300 years.
101 In total, the final dataset had around 25,000 plots and around 44,000 observations. Geographical biases were observed
102 in the compiled dataset (Fig. 1) with North America, Europe and South East of China being well represented, while
103 Africa, Indonesia, and Australia being either underrepresented or not represented at all. The Amazon basin and the West
104 part of Eurasia were relatively well represented. Besides, stand age data were generally collected in locations easily
105 accessible, therefore unmanaged forests in remote areas were very likely less represented than managed forests.

106

107

108

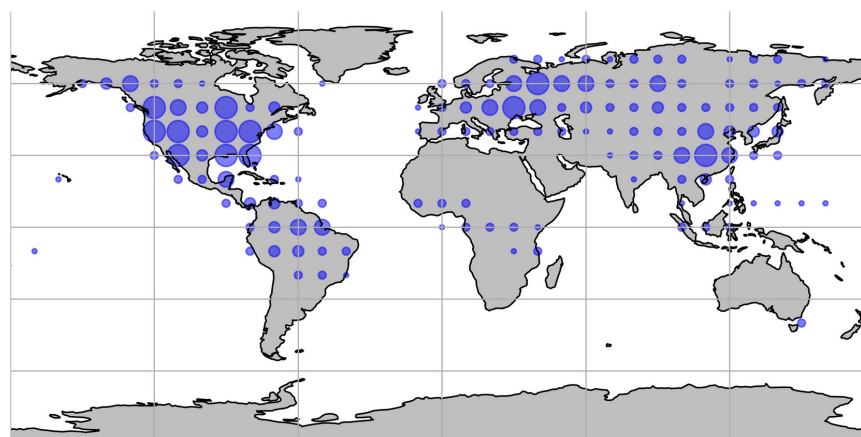
109

110

111

112

113



114

115

116

117

118

119 **Figure 1** Spatial distribution of the forest inventory plots used for the forest age maps. Each dot represents the total
120 number of plots within 10x10 degrees.

121

122 A broad meta-analysis of the compiled dataset (Fig. 2) revealed that the observations covered a large spectrum in the
123 climate-space (Fig. 2A), although in hot and dry regions few plots were collected probably due to the low presence of
124 forest ecosystems in such regions. We further described the age spectrum covered at the regional scale and found that a
125 large spectrum of forest age was cover in North America (Fig. 2B) and Eurasia (Fig. 2C), while in the tropics biases
126 were observed (i.e., large fraction of tropical old-growth forest and relatively young forests) (Fig. 2D).

127

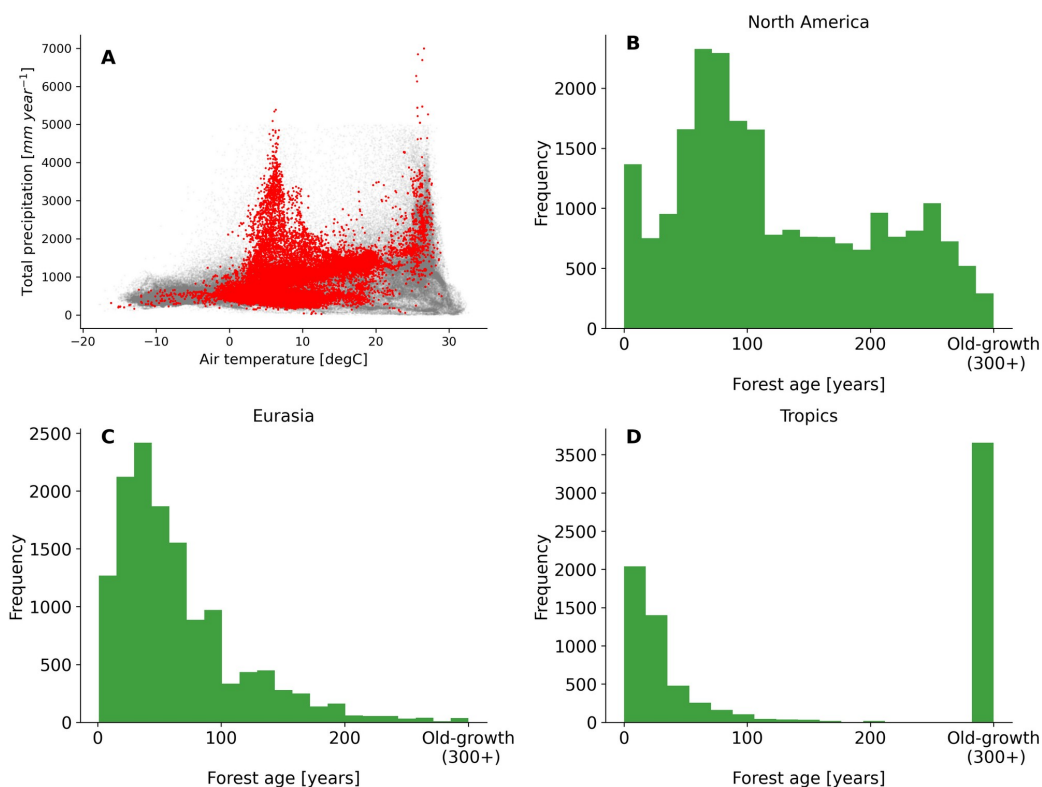
128

129

130



131



133 **Figure 2** Distribution of the forest inventory plots in a climate space defined by air temperature and total annual
134 precipitation (A). Histogram distributions of the forest age observations in North America (B), Eurasia (C) and the
135 tropics (D) are also shown. The grey dots show the global distribution of 0.25° grid-cell forest in climate space defined
136 by air temperature and precipitation, while the red dots show the distribution of the forest inventory data in the same
137 climate space.

138

139 For each forest inventory plot, we extracted bioclimatic variables from the WorldClim version2 (Fick and Hijmans,
140 2017). Table S1 summarizes the list of covariates considered in our study. Two datasets were further created. A non-old-
141 growth forests dataset that contained the plots with a reported stand age estimates ranging from 1 to 299 years-old and a
142 binary dataset reporting whether an observation had an age estimate less than 300 years-old or whether an observation
143 had an age estimate more than or equal to 300 years-old or not reported but considered as old-growth tropical forests
144 (0= non-old-growth forest and 1= old-growth forest).

145 2.2 Feature selection and model training

146 From the set of predictors related to vegetation and climatic conditions (Table S1), we performed a feature ranking with
147 recursive feature elimination (RFE) procedure
148 (https://scikit-learn.org/stable/modules/generated/sklearn.feature_selection.RFE.html) (Guyon et al., 2002) both on the



149 non-old-growth forest and binary datasets. The 10 best covariates selected by the RFE algorithm were further used to
150 train either a Random Forest (RF) regressor algorithm (RFRegressor)
151 (<https://scikit-learn.org/stable/modules/generated/sklearn.ensemble.RandomForestRegressor.html>) or an RF classifier
152 algorithm (Rfclassifier)
153 (<https://scikit-learn.org/stable/modules/generated/sklearn.ensemble.RandomForestClassifier.html>). As such, two distinct
154 models were implemented. The RFRegressor model was used to estimate forest age in the non-old-growth forests
155 dataset, while the Rfclassifier model was used to classify old-growth vs. non-old-growth forests using the binary
156 dataset (0= non-old-growth forest and 1= old-growth forest). The performances of the two models were assessed using
157 leave-one-cluster-out cross-validation to reduce possible spatial auto-correlation between the training and test sets
158 (Ploton et al., 2020). A cluster of plots contained all the plots that were within the same pair of latitude and longitude
159 coordinates rounded to the nearest 10th degree (e.g., latitude= 20 degrees and longitude= 110 degrees) (see Fig. 1). For
160 the RFRegressor model, the root-mean-square error (RMSE), the normalized root-mean-square error (NRMSE) and
161 Nash-Sutcliffe model efficiency coefficient (NSE) were used for assessing the predictive capacity of the model for
162 predicting forest age. For the Rfclassifier model, we reported the precision (i.e., the number of correctly-identified
163 members of a class divided by all the times the model predicted that class), recall (i.e., the number of members of a
164 class that the classifier identified correctly divided by the total number of members in that class) metrics, and F1-score
165 (i.e., combination of precision and recall) for assessing the predictive capacity of the classifier for distinguishing
166 between old-growth and non-old-growth forests. Additionally, we explored functional relationships between the
167 variables selected by the feature selection procedure and stand age in the RFRegressor model by using the Tree SHapley
168 Additive exPlanations (TreeSHAP) algorithm (Lundberg and Lee, 2017; Lundberg et al., 2018). A negative SHAP value
169 for a given variable X translates a negative contribution to the local changes of forest age, and vice-versa.

170 **2.3 Upscaling procedure**

171 To upscale the two models (i.e., Rfclassifier and RFRegressor models) from plot-level data to the global scale, we
172 collected climate grids from the WorldClim dataset (Fick and Hijmans, 2017) and a series of AGB grids *circa* 2010 (i.e.,
173 corrected for tree cover with thresholds of 0%, 10%, 20% and 30%) from the Globbiomass project
174 (<http://globbiomass.org/>). The tree cover correction was done by masking-out the 100-meter pixels in the original AGB
175 product (i.e., 100m resolution) having tree cover estimates (Hansen et al., 2013) below one of the aforementioned tree
176 cover thresholds within a 1km extent. The original filtered AGB maps were further aggregated from 100m to 1km
177 spatial resolution using a bilinear resampling method.

178 The upscaling procedure was done in two steps. First, each 1km pixel was classified either as old-growth or non-old
179 growth forests using the trained Rfclassifier model. Second, the 1km pixels classified as non-old growth were assigned
180 with an age estimate ranging from 0-299 years inferred from the RFRegression model, while the pixels classified as old-
181 growth forest were assigned a default age value of 300 years. In total, four gridded forest age maps with a 1km spatial
182 resolution were obtained using the different aforementioned AGB maps derived from the different tree cover thresholds
183 (hereafter MPI-BGC forest age datasets). From the 1km resolution forest age maps, we also created maps that reflected
184 the fraction of several age classes (0-300+ with decadal resolution) within each 0.5-degree grid cell resolution.



185 **3 Results and discussion**

186 **3.1 Model development and evaluation**

187 We used the 10 most important variables from the set of variables presented in Table S1 identified by the RFE
 188 algorithm procedure for the RFregression and the RFclassifier models (Table 1). This set of selected variables was
 189 further used to train the two models both in the cross-validation analysis and the global upscaling procedure.

190 **Table 1** List of the predictors confirmed as important by the feature selection algorithm for RFregression and the
 191 RFclassifier models. See table S1 for details on the variable names.

Model setup	Vegetation	Climate
RFregression	agb	Isothermality, MaxTemperatureofWarmestMonth, MeanDiurnalRange, MeanTemperatureofWettestQuarter, PrecipitationofWarmestQuarter, PrecipitationofWettestMonth, PrecipitationSeasonality, srad, vapr
RFclassifier	agb	AnnualMeanTemperature, AnnualPrecipitation,Isothermality, MeanTemperatureofColdestQuarter, MeanTemperatureofDriestQuarter, MinTemperatureofColdestMonth, TemperatureAnnualRange, TemperatureSeasonality, vapr

192

193 By assessing the cross-validation results, we found that the RFclassifier model was able to accurately partition old-
 194 growth and non-old-growth forests with precision estimates of 0.81 and 0.99 for old-growth forest and non-old-growth
 195 forests, respectively (Fig. 3A). Furthermore, we found recall values of 0.94 and 0.98 for old-growth forest and non-old-
 196 growth forests, respectively, while we found F1-scores of 0.87 and 0.99 for old-growth forest and non-old-growth
 197 forests, respectively (Fig. 3A). The performance of the RFregression model was relatively high (NSE= 0.60, RMSE=
 198 47.63 years and NRMSE = 51.52%) (Fig. 3B), while the model residuals across 10-degree latitudinal averages were
 199 relatively low (Fig. 3C). However, the quantile-quantile plot depicted biases in both very young and old forests (Fig.
 200 3D). More precisely, the RFregression model slightly overestimated the age estimates of young forests while it
 201 underestimated the age estimates of older forests (i.e., >150 years old) at the plot level. The biases for the very young or
 202 the older forests were probably due to either the properties of the training dataset in which older forests are still largely
 203 underrepresented compared to younger stands (Fig. 2A-C) or the statistical method used (i.e., Random Forests). Such
 204 biases could potentially be propagated from plot level to global scale and have implications in representing the location
 205 of younger and older forests globally.



206
207
208
209
210
211
212
213
214
215
216
217
218
219
220
221
222
223
224
225
226
227
228
229
230
231
232
233
234
235
236
237
238
239
240
241
242

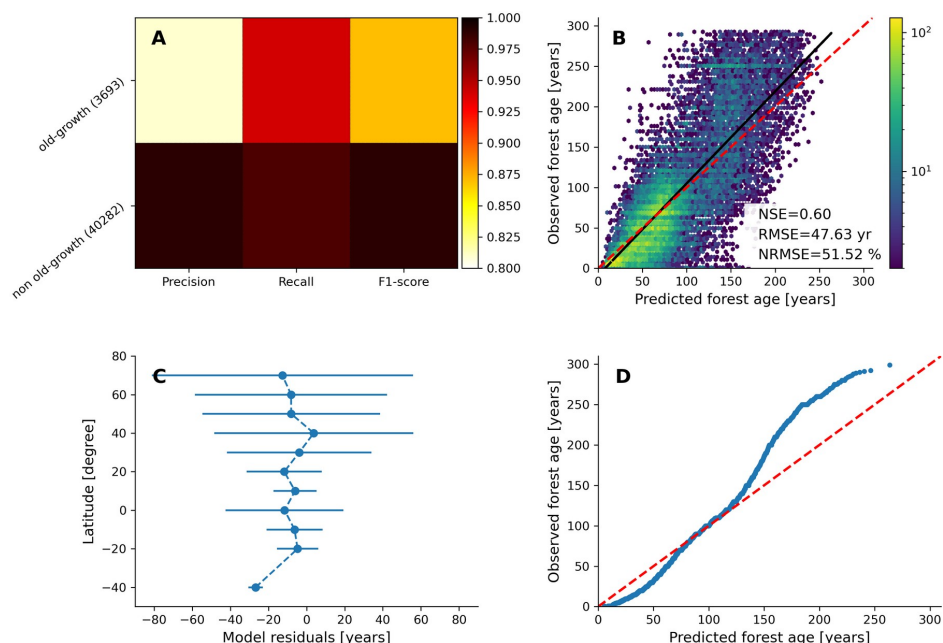


Figure 3 Cross-validated results of the old-forests vs. non-old-forests classification (A) and comparison of predicted vs. observed forest age estimates from the regression model (B). In C, the average model residuals \pm standard deviation within 10-degree latitudinal bins are shown. The quantile-quantile plot (D) is also shown.

We further investigated the variable importance of the selected variables and the functional relationships learned by the RFregression model between forest age and these selected variables. For this, we computed the SHAP values for each predictor to show how each predictor contributes, either positively or negatively, to the forest age estimates. First of all, we observed that *vapr* was the most important variable followed by *agb* and *MeanTemperatureWettestQuarter* (Fig. 4). While it was expected to have biomass (i.e., *agb*) as an important variable in predicting forest age, it was interesting to find that a proxy for atmospheric water demand (i.e., *vapr*) had a strong control on forest age. Such high importance of *vapr* could suggest, for instance, an association between high atmospheric demand for water (i.e., dry conditions) and disturbance intervals (e.g., fire frequency) (Mueller et al., 2020), therefore impacting the age distribution at the plot level.



243

244

245

246

247

248

249

250

251

252

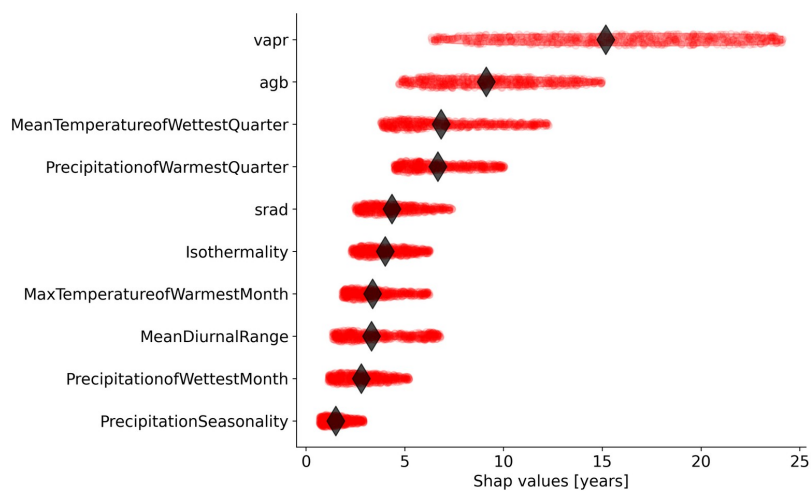
253

254

255

256

257



258

259

260

261

262

263

264

265

266

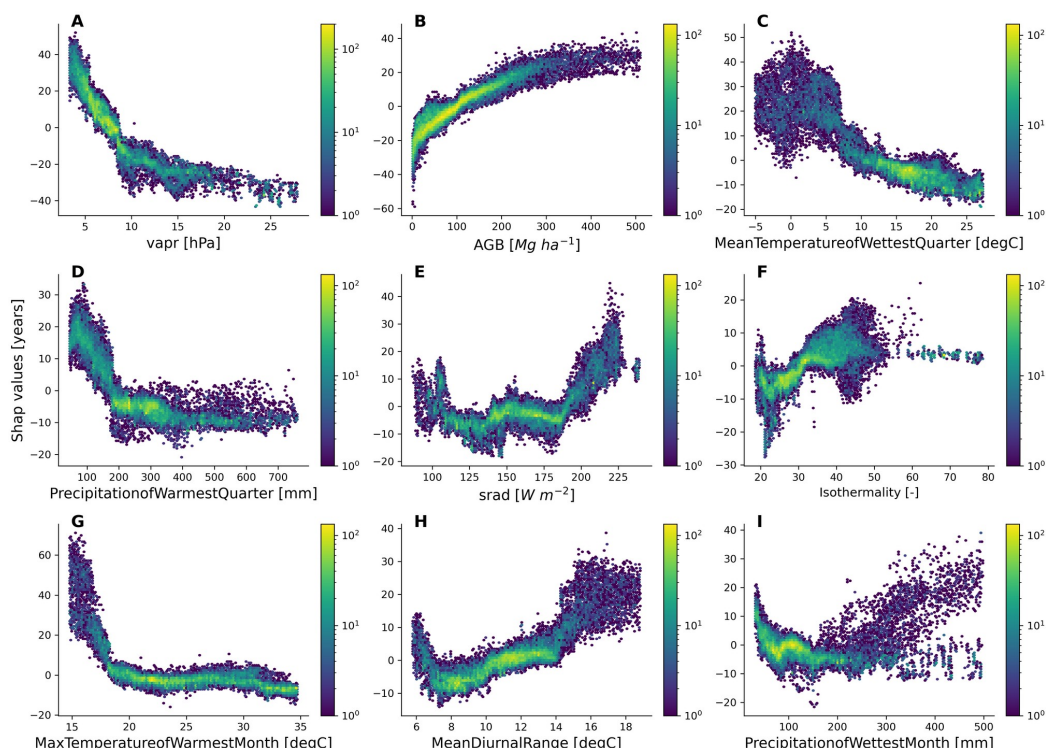
267

268

269

Figure 4 Relative importance of the independent variables selected by the feature selection algorithm in predicting forest age estimates. Each dot represents the absolute SHAP value of one observation. The diamond represents the median value for each variable.

The emergent relationships revealed that an increase in AGB was associated with an increase in the forest age estimates (Fig. 5A). This was expected as older trees have a higher amount of carbon stored in the aboveground components compared to younger forests. The modelled forest age estimates appeared to be also relatively sensitive to the climatic conditions. For instance, we observed that climatic conditions with low water atmospheric demand (i.e., low vapr) (Fig. 5C) promoted older forests as well as conditions with high solar radiation (Fig. 5E), such as in the wet tropics. Finally, we observed that changes in forest age were also associated with air temperature conditions (Fig. 5E-G) and precipitation regimes (Fig. 5H and Fig. 5I).



271 **Figure 5** Emergent relationships between the retrieved SHAP values and the independent variables selected by the
272 feature selection algorithm.

273

274 3.2 Global forest age patterns and regional overview

275 The MPI-BGC forest age product shows a large range of forest age across the globe (Fig. 6). We observed that the most
276 represented age class was the old-growth forests with around 1,1 billion hectares, while a limited fraction of very young
277 forest was observed (i.e., < 10 years old) (Fig. 6A). Not surprisingly, most of the old-growth/undisturbed forests (+300
278 years old) can be found in the Amazon basin (Fig. 6B), the Congo basin (Fig. 6C) and part of the Indonesian peninsula
279 (Fig. 6H), where the minimal human disturbance occurred. A large area occupied by very young forests was found in
280 the Southeast part of China (Fig. 6H), probably due to the implementation of afforestation/reforestation policies as well
281 as natural disturbances (Zhang et al., 2017). Similarly, young and intermediate forests were found in the African tropical
282 dry forests (i.e., Sahel and Miombo regions) (Fig. 6C), where the frequency of the fire regimes is very high resulting in
283 a relatively young age-class structure (Werf et al., 2017). Large scale fires in the North American boreal region also
284 resulted in widespread patches of younger forests as well as a mosaic of stands of different ages since they last burned
285 (Fig. 6G). On the other hand, the unmanaged part of the North American boreal region near the ecotone, where fires are
286 more infrequent, revealed older stands (Fig. 6G). Forests in British Columbia were generally old, although patches of
287 younger forests probably in the early stages of recovery from disturbance were also observed. European forests were in
288 young/intermediate stages of forest succession (Fig. 6E). The increase of harvested forest area (Ceccherini et al., 2020)
289 and considerable afforestation practices (Naudts, et al., 2016) were probably explaining a relatively young to
290 intermediate forest demography as well as a mosaic of different age classes in the European region. The region of



291 Siberia revealed a gradient of younger to older forests going from the South to the North part of the Siberian region
292 (Fig. 6F). Such an observation could suggest different fire regimes between Southern and Northern Siberia. Finally,
293 Australian forests were relatively young in the North part of the country while a mosaic of age class dominated the
294 Southern part of Australia (Fig. 6D). The age patterns observed in the Northern part of Australia somehow correspond
295 to the fact forests are defined as regrowth in this region (Pugh et al., 2019). Yet, it is important to note that the few forest
296 inventory plots in regions such as Australia (Fig. 1) could limit our certainty on the forest age estimates attributed by the
297 statistical approaches due to extrapolation issues.

298
299
300
301
302
303
304

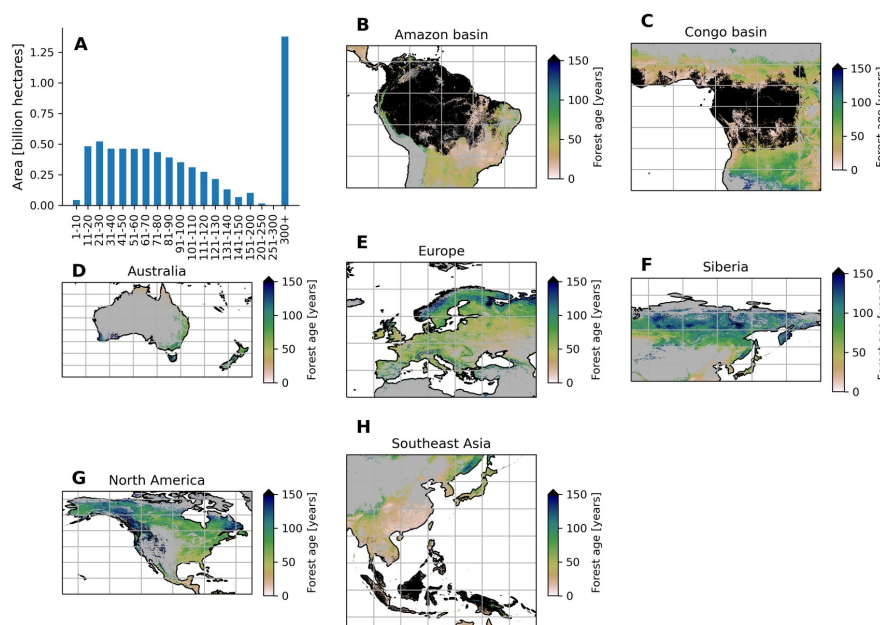


Figure 6 Total area of each age class

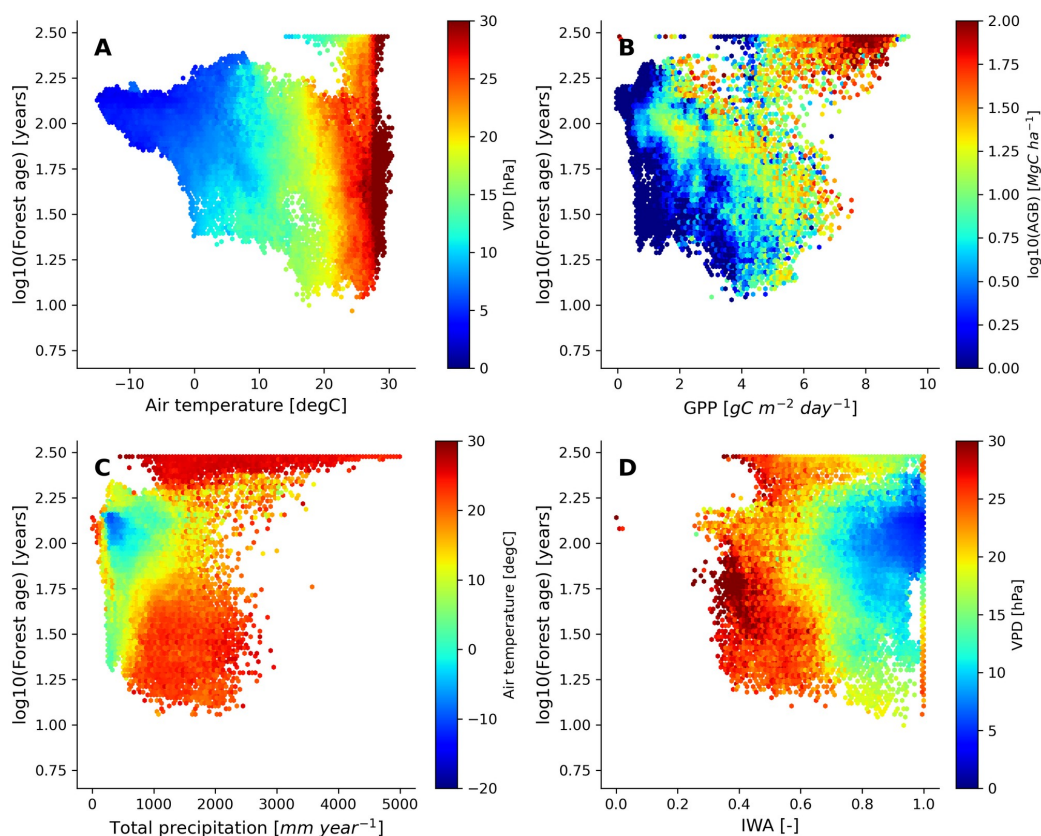
305 globally (A) and close-up examples in the Amazon Basin (B), Congo Basin (C), Australia (D), Europe (E), Siberia (F),
306 North America (G) and Southeast Asia (H). For better visualization, the forest age estimates in the close-up examples
307 (B-H) range from 0 to 150 years-old. The forest age map using a 10% tree cover threshold is shown.
308

309 3.3 Global forest age relationships with atmosphere, hydrosphere and vegetation conditions

310 We further investigated the distribution of the forest demography in the climate and vegetation spaces (Fig. 7).
311 Generally, we observed that with warmer (i.e., air temperature) and drier (i.e., VPD) conditions, forest appeared to be
312 younger with the expectation of old-growth tropical forests located in relatively warm climatic conditions (Fig. 7A).
313 Not surprisingly, we found that most of the old-growth tropical forests were located in regions with high productivity
314 (i.e., high GPP and high biomass) (Fig. 7B), which coincides with our previous results investigating the structure of the
315 statistical model showing that an increase in forest biomass was coupled with an increase in forest age (Fig. 5A). On the
316 other hand, we observed that younger-intermediate forests were more productive than older forests outside the tropical
317 old-growth forest envelope. More precisely, for similar carbon stocks, we found that forest being less productive will
318 tend to belong to an older age class. Mature forests were found in cool temperatures and moderately low precipitation
319 conditions (Fig. 7C), where rates of fast growth but slow decomposition generally drive forest dynamics, therefore
320 where mature forests can potentially be found. Younger stands, on the other hand, were found in relatively warm



321 conditions but in a wide range of precipitation regimes (Fig. 7C). Finally, while a large fraction of young forests were
322 located in regions with low water availability and high water atmospheric demands, we also observed that above a
323 certain threshold of water availability (i.e., > 0.4-0.5), the amount of water available for trees (i.e., IWA) was not
324 directly associated with changes in forest age unlike VPD (Fig. 7D).
325



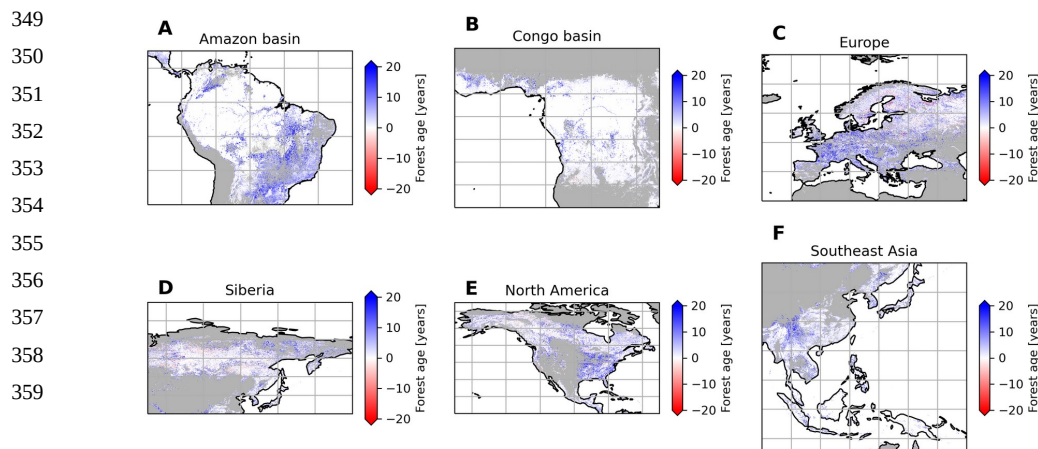
327 **Figure 7** Forest age distribution in the climate, hydrological and productivity spaces defined by air temperature, vapour
328 pressure deficit, total precipitation, soil water availability, GPP and above-ground biomass. The forest age map used
329 here corresponds to a tree cover threshold of 10% aggregated to 0.25 degree using a weighted average of all non-
330 NODATA contributing pixels. GPP is gross primary productivity derived from the FLUXCOM RS+meteo product
331 (Tramontana et al. 2016; Jung et al. 2011; Jung et al. 2020) and IWA is an index for soil water availability (Tramontana
332 et al. 2016). The climatic variables were retrieved from the ERA5-reanalysis data
333 (<https://apps.ecmwf.int/datasets/licences/copernicus/>). For all the climatic variables, we computed an annual mean for
334 the year 2010.

335 3.4 Sensitivity analysis, uncertainties and comparison with previous products

336 We performed a sensitivity analysis using a series of AGB gridded products filtered with different tree cover thresholds
337 to produce different global age products (see method section) (Fig. 8). This analysis showed that in South America,
338 mainly the dry regions were sensitive to the tree cover threshold being applied, with forest age estimates being lower



339 when no tree cover threshold was applied compared to a 30% tree cover correction (Fig. 8A). Similarly, we observed
340 that the dry parts of the Congo basin depicted a sensitivity to the applied tree cover thresholds (Fig. 8B). In Europe, we
341 observed widespread differences between the forest age estimated without a tree cover correction and with a tree cover
342 correction (Fig. 8C). Generally, forest age estimates were higher when the 30% tree cover correction was applied. In
343 Siberia (Fig. 8D), North America (Fig. 8E) and Southeast Asia (Fig. 8F), there were also large patches of forest where
344 correcting the biomass maps with a tree cover threshold led to substantial differences in the age estimates. Overall, such
345 observations were expected as mosaic vegetation, due to management practices or disturbance regimes, in the dry
346 tropics (forest/grassland/shrubland), in Europe (forests/croplands) and Northeast of the United States (forests/croplands)
347 are largely represented within a 1km grid cell, which could explain the sensitivity of the forest age estimates to tree
348 cover thresholds in these regions.



360 **Figure 8** Sensitivity of the presented age product using 30% tree cover correction thresholds or no tree cover correction.
361 The differences between the age estimates derived from a forest biomass product using a 30% tree cover correction and
362 the age estimates derived from a forest biomass product not using a tree cover correction are shown. Blue colour means
363 that the age estimates are higher with the 30% tree cover correction than without correction, while the red colour means
364 that the age estimates are lower with the 30% tree cover correction than without correction.

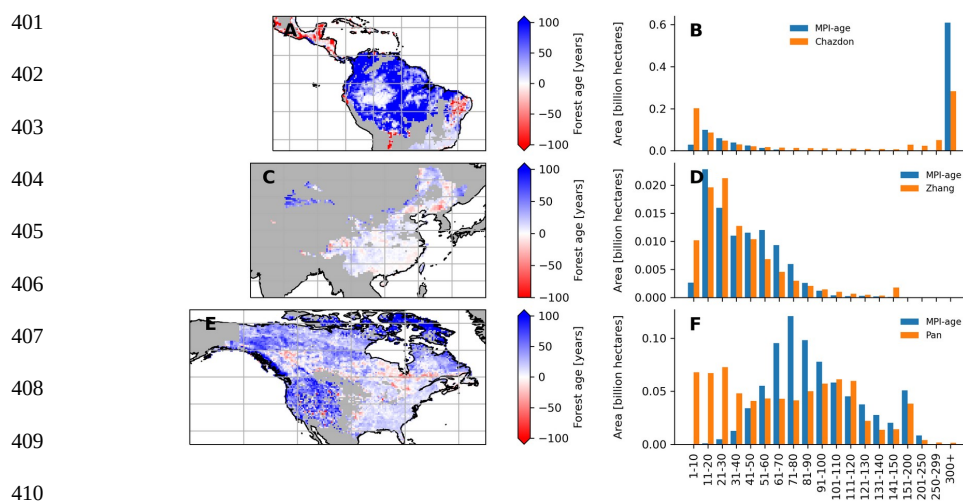
365

366 Besides, we explored uncertainties associated with the two statistical models used for the upscaling procedure (Fig. S1,
367 Fig. S2 and Fig. S3). First, we observed that the RFclassifier model had overall very high probabilities to classify a non-
368 old-growth forest pixel when being classified as a non-old-growth forest (Fig. S1), and vice-versa (Fig. S2), suggesting
369 relatively high confidence in the partitioning between old-growth and non-old-growth forests in the MPI-BGC forest
370 age product. The regions at the edge of the Amazon and the Congo basins appeared to have the lowest confidence in
371 classifying old-growth vs. non-old-growth forests (Fig. S1A, Fig. S1B and Fig. S2) with a probability close to 0.5. On
372 the other hand, we observed relatively high probabilities for classifying non-old-growth forests in Europe (Fig. S1C),
373 Siberia (Fig. S1D), North America (Fig. S1E) and Southeast Asia (Fig. S1F). We also provided uncertainties in
374 predicting forest age estimates by retrieving the 25%, 50%, and 75% quantile predictions from the RFregressor model
375 for computing the inter-quantile range (IQR, quantile 75% - quantile 25%) divided by the median (i.e., quantile 50%) of
376 the forest age estimates (IQR/median) (Fig. S3). While in Europe (Fig. S3C), China (Fig. S3F) and the Eastern United
377 States (Fig. S3E) the IQR/median estimates were relatively low, we observed high IQR/median estimates in Northern



378 North American regions (Fig. S3E) as well as in large patches of Siberia (Fig. S3D) and the dry tropics (Fig. S3A and
 379 Fig. S3F).

380 We further compared the spatial patterns of the MPI-BGC forest age dataset with a series of independent regional and
 381 global forest age products (Chazdon et al., 2016; Pan et al., 2011; Poulter et al., 2019; Zhang et al., 2017) (Fig. 9 and
 382 Fig. 10). In the Amazon basin, we found that the MPI-BGC forest age product depicted widespread higher forest age
 383 estimates (i.e., blue colour) than the Chazdon et al. (2016) dataset (Fig. 9A), resulting in a substantially bigger area of
 384 tropical old-growth forest in the MPI-BGC forest age product (Fig. 9B). On the other hand, we observed lower forest
 385 age estimates in the regions of Rio Grande Do Norte and Paraíba in the MPI-BGC forest age product (i.e., red colour).
 386 Such disagreement between the two products could be related not only to the different methods used to infer forest age
 387 (i.e., statistical method vs. age-AGB chronosequence approach for the MPI-BGC forest age and the Chazdon products,
 388 respectively) but also to the uncertainties of the RFclassifier for classifying old-growth vs. non-old-growth forests in
 389 this region (Fig. S1 and Fig. S2). Similarly, the presented product and the Pan et al. (2011) dataset revealed widespread
 390 discrepancies in the North American region, particularly in the Western part of the United States and the North
 391 American boreal forests (Fig. 8E). More precisely, the Pan et al. (2011) dataset had a higher fraction of young forest
 392 patches than the MPI-BGC forest age product (Fig. 9F). Methodological differences between the Pan et al. (2011) and
 393 the MPI-BGC forest age datasets could explain such differences. While forest inventory, fire polygon data and remote
 394 sensing and a multi-stage approach were used to retrieve forest age estimates in the Pan et al. (2011) dataset, the MPI-
 395 BGC forest age product relied on forest inventory and climate data as well as statistical methods. Additionally, forest
 396 inventory plots used to derive the MPI-BGC forest age product were relatively sparse in Canada (Fig. 1), which might
 397 limit the statistical methods used for the MPI-BGC forest age product to predict realistic forest age estimates (i.e.,
 398 extrapolation issues). Finally, the forest age estimates of the MPI-BGC forest age product in China were rather
 399 consistent with the Zhang et al. (2017) dataset (Fig. 9C). The area distribution across age classes of the two products
 400 appeared to have a relatively good agreement in China (Fig. 9D).



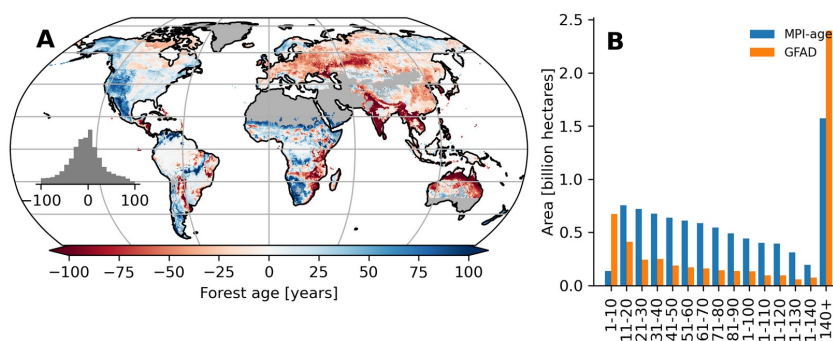
411 **Figure 9** Comparison between the forest age dataset from this study and independent forest age dataset: Amazon basin
 412 (A and B), China (C and D) and North America (E and F). For a fair comparison with the independent age datasets, the
 413 MPI-BGC forest age map used here is the one without tree cover correction applied to the AGB dataset. Differences



414 were computed using weighted age estimates from the fraction of the decadal age classes within each 0.5-degree grid
415 cell resolution.

416 We also found large and widespread discrepancies between the MPI-BGC forest age dataset and the global forest age
417 dataset (GFAD) (Poulter et al., 2019) (Fig. 10). Overall, the GFAD product had both higher fractions of very young
418 forests and old forests (Fig. 10B). Because the GFAD used a different AGB product for the pan-tropical region and
419 mainly relied on coarse national forest inventory data for the Northern hemisphere, widespread differences were
420 expected between the GFAD and the MPI-BGC forest age maps. For instance, the MPI-BGC forest age dataset depicted
421 older forests in the Western part of the United States (i.e., blue colour), while it showed younger forests across Europe
422 than the GFAD product (Fig. 10A). Differences were also apparent in the dry tropics, where the MPI-BGC forest age
423 dataset showed younger forests than the GFAD product, particularly in the Miombo regions. Such observations could be
424 explained by the integration of MODIS fire information in the GFAD forest age dataset. As such, we adjusted the MPI-
425 BGC forest age dataset with the forest age product inferred from the MCD45A1 MODerate-resolution Imaging
426 Spectroradiometer (MODIS) fire product at 1 km resolution (Giglio et al., 2018, Poulter et al., 2019), which was used in
427 the GFAD product. In this MODIS-age product, forest age was determined as the last time since a fire event occurred
428 within a grid cell for the period 2000-2015, thereby assuming that the entire pixel was burned down. For instance, forest
429 age within a 1 km grid cell was 5 years old if the last time a fire occurred within this grid cell was in 2010. When
430 adjusting the MPI-BGC forest age dataset with the MODIS-age product, the latter took precedence over the former
431 dataset. As expected, we observed a higher fraction of younger forest in the adjusted MPI-BGC forest age dataset (Fig.
432 S4B), although large discrepancies between the two products remained when comparing the weighted average forest
433 age estimates at the pixel level (Fig. S4A).

434
435
436
437
438
439
440
441
442
443
444



445 **Figure 10** Difference between the forest age estimates derived from the MPI-BGC forest age product and the GFAD
446 product. Differences were computed using weighted age estimates from the fraction of the decadal age classes within
447 each 0.5-degree grid cell resolution.

448 4 Data availability

449 The dataset of the different forest age products presented in this study can be downloaded from the Data Portal of the
450 Max Planck Institute for Biogeochemistry at <https://doi.org/10.17871/ForestAgeBGL2021> (Besnard et al., 2021). For
451 anonymous access during review, the data are available at <https://nextcloud.bgc-jena.mpg.de/s/Xwt8AdkHkgL3Ttc>.



452 **5 Conclusion**

453 We presented a new forest age dataset derived from forest inventory, biomass, climate and remote sensing data.
454 Generally, the statistical model used to create the gridded age datasets had a relatively good capacity to predict forest
455 age estimates at plot level (precision of 0.81 and 0.99 for classifying old-growth and non-old-growth, respectively and
456 NSE of 0.6 for predicting non-old-growth forests), while biases were observed particularly when predicting older
457 forests. The functional relationships between biomass and forest age learned by the statistical models appeared to agree
458 with forest age theory and the role of environmental/climate in modulating the relationship. The proposed gridded
459 datasets allowed us to assess the global patterns of forest age and provided insights into regional forest demography. For
460 instance, relatively young-intermediate forests were observed in Europe and China where management practices and
461 afforestation/reforestation activities are predominant. We could also demonstrate that old forests are largely represented
462 in very wet and warm regions as well as in very cold regions. However, the comparison of the MPI-BGC forest age
463 product with independent forest age datasets revealed large discrepancies between them, suggesting high uncertainties
464 in mapping forest demography globally. Overall, this forest age product provides a new source of information related to
465 disturbance history and forest regrowth, which is key to achieve a better understanding of the location of the forest
466 carbon sinks and sources.

467

468 **Author contributions**

469 SB and NC designed the study. SB conducted analysis and wrote the paper under the direction of NC. SB, NC, SK, JG,
470 and UW collected and harmonized the forest inventories datasets. BP, BH, JK, and AN provided data for the analysis.
471 All authors contributed to the discussions and interpretation of the results and the writing of the paper.

472

473 **Competing interests**

474 The authors declare that they have no conflict of interest.

475

476 **Acknowledgments**

477 We would like to thank all the initiatives aiming to collect forest inventory plots. We thank the members of the
478 Biogeochemical Integration Department at the Max Planck Institute for Biogeochemistry for providing feedback on the
479 presented results. We acknowledge support by the European Union through the BIOMASCAT
480 (<https://eo4society.esa.int/projects/biomascats/>) and VERIFY (776810) (<https://cordis.europa.eu/project/id/776810>)
481 projects.

482 **References**

- 483 Álvarez-Dávila, E., L. Cayuela, S. González-Caro, A. M. Aldana, P. R. Stevenson, O. Phillips, Á. Cogollo, M. C.
484 Peñuela, P. v. Hildebrand, E. Jiménez, O. Melo, A. C. Londoño-Vega, I. Mendoza, O. Velásquez, F. Fernández, M.
485 Serna, C. Velázquez-Rua, D. Benítez, and J. M. Rey-Benayas (2017). “Forest biomass density across large climate
486 gradients in northern South America is related to water availability but not with temperature”. PLOS ONE 12.3,
487 e0171072.
- 488 Amiro, B. D., A. G. Barr, J. G. Barr, T. A. Black, R. Bracho, M. Brown, J. Chen, K. L. Clark, K. J. Davis, A. R. Desai,
489 S. Dore, V. Engel, J. D. Fuentes, A. H. Goldstein, M. L. Goulden, T. E. Kolb, M. B. Lavigne, B. E. Law, H. A. Margolis,



- 490 T. Martin, J. H. McCaughey, L. Misson, M. Montes-Helu, A. Noormets, J. T. Randerson, G. Starr, and J. Xiao (2010).
491 “Ecosystem carbon dioxide fluxes after disturbance in forests of North America”. *Journal of Geophysical Research:*
492 *Biogeosciences* 115.G4.
- 493 Anderson-Teixeira, K. J., M. M. H. Wang, J. C. McGarvey, V. Herrmann, A. J. Topley, B. Bond- Lamberty, and D. S.
494 LeBauer (2018). “ForC: a global database of forest carbon stocks and fluxes”. *Ecology* 99.6, 1507.
- 495 Anderson-Teixeira, K. J., M. M. H. Wang, J. C. McGarvey, and D. S. LeBauer (2016). “Carbon dynamics of mature and
496 regrowth tropical forests derived from a pantropical database (TropForC-db)”. *Global Change Biology* 22.5, 1690–
497 1709.
- 498 Baker, T. R., D. M. V. Díaz, V. C. Moscoso, G. Navarro, A. Monteagudo, R. Pinto, K. Cangani, N. M. Fyllas, G. L.
499 Gonzalez, W. F. Laurance, S. L. Lewis, J. Lloyd, H. t. Steege, J. W. Terborgh, and O. L. Phillips (2016). “Consistent,
500 small effects of treefall disturbances on the composition and diversity of four Amazonian forests”. *Journal of Ecology*
501 104.2, 497–506.
- 502 Bar-On, YM, Phillips, R., & Milo, R. (2018). The biomass distribution on Earth. *Proceedings of the National Academy*
503 *of Sciences*, 115 (25), 6506-6511.
- 504 Besnard, S., Koirala, S., Santoro, M., Weber, U., Nelson, J., Gütter, J, Herault, B., Kassi, J., N'Guessan, A., Neigh, C.,
505 Poulter, B., Zhang, T., and Carvarhais, N. (2021). The MPI-BGC global forest age datasets, MPI-BGC,
506 <https://doi.org/10.17871/ForestAgeBGI.2021>.
- 507 Besnard, S., N. Carvalhais, M. A. Arain, A. Black, S. d. Bruin, N. Buchmann, A. Cescatti, J. Chen, J. G. P. W. Clevers,
508 A. R. Desai, C. M. Gough, K. Havrankova, M. Herold, L. Hörtnagl, M. Jung, A. Knohl, B. Kruijt, L. Krupkova, B. E.
509 Law, A. Lindroth, A. Noormets, O. Roupsard, R. Steinbrecher, A. Varlagin, C. Vincke, and M. Reichstein (2018).
510 “Quantifying the effect of forest age in annual net forest carbon balance”. *Environmental Research Letters* 13.12,
511 124018.
- 512 Birdsey, R., K. Pregitzer, and A. Lucier (2006). “Forest carbon management in the United States: 1600-2100”. *Journal*
513 *of Environmental Quality* 35.4, 1461–1469.
- 514 Bowman, D. M. J. S., J. K. Balch, P. Artaxo, W. J. Bond, J. M. Carlson, M. A. Cochrane, C. M. D’Antonio, R. S.
515 DeFries, J. C. Doyle, S. P. Harrison, F. H. Johnston, J. E. Keeley, M. A. Krawchuk, C. A. Kull, J. B. Marston, M. A.
516 Moritz, I. C. Prentice, C. I. Roos, A. C. Scott, T. W. Swetnam, G. R. v. d. Werf, and S. J. Pyne (2009). “Fire in the Earth
517 System”. *Science* 324.5926, 481–484.
- 518 Buitenwerf, R., B. Sandel, S. Normand, A. Mimet, and J.-C. Svenning (2018). “Land surface greening suggests
519 vigorous woody regrowth throughout European semi-natural vegetation”. *Global Change Biology* 24.12, 5789–5801.
- 520 Burrill, Elizabeth A.; Wilson, Andrea M.; Turner, Jeffery A.; Pugh, Scott A.; Menlove, James; Christiansen, Glenn;
521 Conkling, Barbara L.; David, Winnie. 2018. The Forest Inventory and Analysis Database: database description and user
522 guide version 8.0 for Phase 2. U.S. Department of Agriculture, Forest Service. 946 p.
- 523 Ceccherini, G., Duveiller, G., Grassi, G., Lemoine, G., Avitabile, V., Pilli, R., & Cescatti, A. (2020). Abrupt increase in
524 harvested forest area over Europe after 2015. *Nature*, 583(7814), 72-77.
- 525 Ciais, P., A. J. Dolman, A. Bombelli, R. Duren, A. Peregón, P. J. Rayner, C. Miller, N. Gobron, G. Kinderman, G.
526 Marland, N. Gruber, F. Chevallier, R. J. Andres, G. Balsamo, L. Bopp, F.-M. Bréon, G. Broquet, R. Dargaville, T. J.



- 527 Battin, A. Borges, H. Bovensmann, M. Buchwitz, J. Butler, J. G. Canadell, R. B. Cook, R. DeFries, R. Engelen, K. R.
528 Gurney, C. Heinze, M. Heimann, A. Held, M. Henry, B. Law, S. Luyssaert, J. Miller, T. Moriyama, C. Moulin, R. B.
529 Myneni, C. Nussli, M. Obersteiner, D. Ojima, Y. Pan, J.-D. Paris, S. L. Piao, B. Poulter, S. Plummer, S. Quegan, P.
530 Raymond, M. Reichstein, L. Rivier, C. Sabine, D. Schimel, O. Tarasova, R. Valentini, R. Wang, G. van der Werf, D.
531 Wickland, M. Williams, and C. Zehner (2014). “Current systematic carbon-cycle observations and the need for
532 implementing a policy-relevant carbon observing system”. *Biogeosciences* 11.13, 3547–3602.
- 533 Chazdon, R. L., E. N. Broadbent, D. M. A. Rozendaal, F. Bongers, A. M. A. Zambrano, T. M. Aide, P. Balvanera, J. M.
534 Becknell, V. Boukili, P. H. S. Brancalion, D. Craven, J. S. Almeida-Cortez, G. A. L. Cabral, B. d. Jong, J. S. Denslow,
535 D. H. Dent, S. J. DeWalt, J. M. Dupuy, S. M. Durán, M. M. Espírito-Santo, M. C. Fandino, R. G. César, J. S. Hall, J. L.
536 Hernández-Stefanoni, C. C. Jakovac, A. B. Junqueira, D. Kennard, S. G. Letcher, M. Lohbeck, M. Martínez-Ramos, P.
537 Massoca, J. A. Meave, R. Mesquita, F. Mora, R. Muñoz, R. Muscarella, Y. R. F. Nunes, S. Ochoa-Gaona, E. Orihuela-
538 Belmonte, M. Peña-Claros, E. A. Pérez-García, D. Piotto, J. S. Powers, J. Rodríguez-Velazquez, I. E. Romero-Pérez, J.
539 Ruíz, J. G. Saldarriaga, A. Sanchez-Azofeifa, N. B. Schwartz, M. K. Steininger, N. G. Swenson, M. Uriarte, M. v.
540 Breugel, H. v. d. Wal, M. D. M. Veloso, H. Vester, I. C. G. Vieira, T. V. Bentos, G. B. Williamson, and L. Poorter (2016).
541 “Carbon sequestration potential of second-growth forest regeneration in the Latin American tropics”. *Science Advances*
542 2.5, e1501639.
- 543 Cook-Patton, S. C., Leavitt, S. M., Gibbs, D., Harris, N. L., Lister, K., Anderson-Teixeira, K. J., ... & Griscom, B. W.
544 (2020). Mapping carbon accumulation potential from global natural forest regrowth. *Nature*, 585(7826), 545–550.
- 545 Fick, S. E. and R. J. Hijmans (2017). “WorldClim 2: new 1-km spatial resolution climate surfaces for global land areas”.
546 *International Journal of Climatology* 37.12, 4302–4315.
- 547 Hansen, M. C., P. V. Potapov, R. Moore, M. Hancher, S. A. Turubanova, A. Tyukavina, D. Thau, S. V. Stehman, S. J.
548 Goetz, T. R. Loveland, A. Kommareddy, A. Egorov, L. Chini, C. O. Justice, and J. R. G. Townshend (2013). “High-
549 Resolution Global Maps of 21st-Century Forest Cover Change”. *Science* 342.6160, 850–853.
- 550 Huang, C., S. N. Goward, J. G. Masek, N. Thomas, Z. Zhu, and J. E. Vogelmann (2010). “An automated approach for
551 reconstructing recent forest disturbance history using dense Landsat time series stacks”. *Remote Sensing of*
552 *Environment* 114.1, 183–198.
- 553 Giglio, L., L. Boschetti, D. P. Roy, M. L. Humber, and C. O. Justice (2018). “The Collection 6 MODIS burned area
554 mapping algorithm and product”. *Remote Sensing of Environment* 217, 72–85.
- 555 Guyon, I., Weston, J., Barnhill, S., and Vapnik, V. (2002). “Gene selection for cancer classification using support vector
556 machines”, *Mach. Learn.*, 46(1-3), 389–422.
- 557 Irvine, J., B. E. Law, and M. R. Kurpius (2005). “Coupling of canopy gas exchange with root and rhizosphere
558 respiration in a semi-arid forest”. *Biogeochemistry* 73.1, 271–282.
- 559 Johnson, M. O., D. Galbraith, M. Gloor, H. D. Deurwaerder, M. Guimberteau, A. Rammig, K. Thonicke, H. Verbeeck,
560 C. v. Randow, A. Monteagudo, O. L. Phillips, R. J. W. Brienen, T. R. Feldpausch, G. L. Gonzalez, S. Fauset, C. A.
561 Quesada, B. Christoffersen, P. Ciais, G. Sampaio, B. Kruijt, P. Meir, P. Moorcroft, K. Zhang, E. Alvarez-Davila, A. A. d.
562 Oliveira, I. Amaral, A. Andrade, L. E. O. C. Aragao, A. Araujo-Murakami, E. J. M. M. Arets, L. Arroyo, G. A. Aymard,
563 C. Baraloto, J. Barroso, D. Bonal, R. Boot, J. Camargo, J. Chave, A. Cogollo, F. C. Valverde, A. C. L. d. Costa, A. D.



- 564 Fiore, L. Ferreira, N. Higuchi, E. N. Honorio, T. J. Killeen, S. G. Laurance, W. F. Laurance, J. Licona, T. Lovejoy, Y.
565 Malhi, B. Marimon, B. H. Marimon, D. C. L. Matos, C. Mendoza, D. A. Neill, G. Pardo, M. Peña-Claros, N. C. A.
566 Pitman, L. Poorter, A. Prieto, H. Ramirez-Angulo, A. Roopsind, A. Rudas, R. P. Salomao, M. Silveira, J. Stropp, H. t.
567 Steege, J. Terborgh, R. Thomas, M. Toledo, A. Torres-Lezama, G. M. F. v. d. Heijden, R. Vasquez, I. C. G. Vieira, E.
568 Vilanova, V. A. Vos, and T. R. Baker (2016). “Variation in stem mortality rates determines patterns of above-ground
569 biomass in Amazonian forests: implications for dynamic global vegetation models”. *Global Change Biology* 22.12,
570 3996–4013.
- 571 Johnson, D. W. and P. S. Curtis (2001). “Effects of forest management on soil C and N storage: meta analysis”. *Forest*
572 *Ecology and Management* 140.2, 227–238.
- 573 Jung, M., Schwalm, C., Migliavacca, M., Walther, S., Camps-Valls, G., Koirala, S., ... & Reichstein, M. (2020). Scaling
574 carbon fluxes from eddy covariance sites to globe: synthesis and evaluation of the FLUXCOM approach.
575 *Biogeosciences*, 17(5), 1343-1365.
- 576 Jung, M., M. Reichstein, H. A. Margolis, A. Cescatti, A. D. Richardson, M. A. Arain, A. Arneeth, C. Bernhofer, D. Bonal,
577 J. Chen, D. Gianelle, N. Gobron, G. Kiely, W. Kutsch, G. Lasslop, B. E. Law, A. Lindroth, L. Merbold, L. Montagnani,
578 E. J. Moors, D. Papale, M. Sottocornola, F. Vaccari, and C. Williams (2011). “Global patterns of land-atmosphere fluxes
579 of carbon dioxide, latent heat, and sensible heat derived from eddy covariance, satellite, and meteorological
580 observations”. *Journal of Geophysical Research: Biogeosciences* 116.G3.
- 581 Kennedy, R. E., Z. Yang, and W. B. Cohen (2010). “Detecting trends in forest disturbance and recovery using yearly
582 Landsat time series: 1. LandTrendr — Temporal segmentation algorithms”. *Remote Sensing of Environment* 114.12,
583 2897–2910.
- 584 Lewis, S. L., B. Sonké, T. Sunderland, S. K. Begne, G. Lopez-Gonzalez, G. M. F. van der Heijden, O. L. Phillips, K.
585 Affum-Baffoe, T. R. Baker, L. Banin, J.-F. Bastin, H. Beeckman, P. Boeckx, J. Bogaert, C. De Cannière, E. Chezeaux,
586 C. J. Clark, M. Collins, G. Djagbletey, M. N. K. Djuikouo, V. Droissart, J.-L. Doucet, C. E. N. Ewango, S. Fauset, T. R.
587 Feldpausch, E. G. Foli, J.-F. Gillet, A. C. Hamilton, D. J. Harris, T. B. Hart, T. de Haulleville, A. Hladik, K. Hufkens, D.
588 Huygens, P. Jeanmart, K. J. Jeffery, E. Kearsley, M. E. Leal, J. Lloyd, J. C. Lovett, J.-R. Makana, Y. Malhi, A. R.
589 Marshall, L. Ojo, K. S.-H. Peh, G. Pickavance, J. R. Poulsen, J. M. Reitsma, D. Sheil, M. Simo, K. Steppe, H. E.
590 Taedoung, J. Talbot, J. R. D. Taplin, D. Taylor, S. C. Thomas, B. Toirambe, H. Verbeeck, J. Vleminckx, L. J. T. White,
591 S. Willcock, H. Woell, and L. Zomagho (2013). “Above-ground biomass and structure of 260 African tropical forests”.
592 *Philosophical Transactions of the Royal Society B: Biological Sciences* 368.1625, 20120295.
- 593 Liu, S., B. Bond-Lamberty, J. A. Hicke, R. Vargas, S. Zhao, J. Chen, S. L. Edburg, Y. Hu, J. Liu, A. D. McGuire, J.
594 Xiao, R. Keane, W. Yuan, J. Tang, Y. Luo, C. Potter, and J. Oeding (2011). “Simulating the impacts of disturbances on
595 forest carbon cycling in North America: Processes, data, models, and challenges”. *Journal of Geophysical Research:*
596 *Biogeosciences* 116.G4.
- 597 Lundberg, S. M., Erion, G. G., & Lee, S. I. (2018). Consistent individualized feature attribution for tree ensembles.
598 arXiv preprint arXiv:1802.03888.
- 599 Lundberg, S. M., & Lee, S. I. (2017). A unified approach to interpreting model predictions. In *Advances in neural*
600 *information processing systems* (pp. 4765-4774).



- 601 Mitchard, E. T. A., T. R. Feldpausch, R. J. W. Brienen, G. Lopez-Gonzalez, A. Monteagudo, T. R. Baker, S. L. Lewis, J.
602 Lloyd, C. A. Quesada, M. Gloor, H. t. Steege, P. Meir, E. Alvarez, A. Araujo-Murakami, L. E. O. C. Aragão, L. Arroyo,
603 G. Aymard, O. Banki, D. Bonal, S. Brown, F. I. Brown, C. E. Cerón, V. C. Moscoso, J. Chave, J. A. Comiskey, F.
604 Cornejo, M. C. Medina, L. D. Costa, F. R. C. Costa, A. D. Fiore, T. F. Domingues, T. L. Erwin, T. Frederickson, N.
605 Higuchi, E. N. H. Coronado, T. J. Killeen, W. F. Laurance, C. Levis, W. E. Magnusson, B. S. Marimon, B. H. M. Junior,
606 I. M. Polo, P. Mishra, M. T. Nascimento, D. Neill, M. P. N. Vargas, W. A. Palacios, A. Parada, G. P. Molina, M. Peña-
607 Claros, N. Pitman, C. A. Peres, L. Poorter, A. Prieto, H. Ramirez-Angulo, Z. R. Correa, A. Roopsind, K. H. Roucoux, A.
608 Rudas, R. P. Salomão, J. Schiatti, M. Silveira, P. F. d. Souza, M. K. Steininger, J. Stropp, J. Terborgh, R. Thomas, M.
609 Toledo, A. Torres-Lezama, T. R. v. Andel, G. M. F. v. d. Heijden, I. C. G. Vieira, S. Vieira, E. Vilanova-Torre, V. A. Vos,
610 O. Wang, C. E. Zartman, Y. Malhi, and O. L. Phillips (2014). “Markedly divergent estimates of Amazon forest carbon
611 density from ground plots and satellites”. *Global Ecology and Biogeography* 23.8, 935–946.
- 612 Moore, D. J. P., N. A. Trahan, P. Wilkes, T. Quaife, B. B. Stephens, K. Elder, A. R. Desai, J. Negron, and R. K. Monson
613 (2013). “Persistent reduced ecosystem respiration after insect disturbance in high elevation forests”. *Ecology Letters*
614 16.6, 731–737.
- 615 N’Guessan, A. E., J. K. N’dja, O. N. Yao, B. H. K. Amani, R. G. Z. Gouli, C. Piponiot, I. C. Zo-Bi, and B. Hérault
616 (2019). “Drivers of biomass recovery in a secondary forested landscape of West Africa”. *Forest Ecology and*
617 *Management* 433, 325–331.
- 618 Naudts, K., Chen, Y., McGrath, M. J., Ryder, J., Valade, A., Otto, J., & Luysaert, S. (2016). Europe’s forest
619 management did not mitigate climate warming. *Science*, 351(6273), 597-600.
- 620 Odum, E. P. (1969). “The Strategy of Ecosystem Development”. *Science* 164.3877, 262–270.
- 621 Pan, Y., J. M. Chen, R. Birdsey, K. McCullough, L. He, and F. Deng (2011). “Age structure and disturbance legacy of
622 North American forests”. *Biogeosciences* 8.3, 715–732.
- 623 Piponiot, C., Derroire, G., Descroix, L., Mazzei, L., Rutishauser, E., Sist, P., & Hérault, B. (2018). Assessing timber
624 volume recovery after disturbance in tropical forests—a new modelling framework. *Ecological Modelling*, 384, 353-369.
- 625 Ploton, P., Mortier, F., Réjou-Méchain, M., Barbier, N., Picard, N., Rossi, V., ... & Pélissier, R. (2020). Spatial validation
626 reveals poor predictive performance of large-scale ecological mapping models. *Nature communications*, 11 (1), 1-11.
- 627 Poorter, L., F. Bongers, T. M. Aide, A. M. Almeyda Zambrano, P. Balvanera, J. M. Becknell, V. Boukili, P. H. S.
628 Brancalion, E. N. Broadbent, R. L. Chazdon, D. Craven, J. S. de Almeida- Cortez, G. A. L. Cabral, B. H. J. de Jong, J.
629 S. Denslow, D. H. Dent, S. J. DeWalt, J. M. Dupuy, S. M. Durán, M. M. Espírito-Santo, M. C. Fandino, R. G. César, J.
630 S. Hall, J. L. Hernandez-Stefanoni, C. C. Jakovac, A. B. Junqueira, D. Kennard, S. G. Letcher, J.-C. Licona, M.
631 Lohbeck, E. Marín-Spiotta, M. Martínez-Ramos, P. Massoca, J. A. Meave, R. Mesquita, F. Mora, R. Muñoz, R.
632 Muscarella, Y. R. F. Nunes, S. Ochoa-Gaona, A. A. de Oliveira, E. Orihuela-Belmonte, M. Peña-Claros, E. A. Pérez-
633 García, D. Piotto, J. S. Powers, J. Rodríguez-Velázquez, I. E. Romero-Pérez, J. Ruíz, J. G. Saldarriaga, A. Sanchez-
634 Azofeifa, N. B. Schwartz, M. K. Steininger, N. G. Swenson, M. Toledo, M. Uriarte, M. van Breugel, H. van der Wal, M.
635 D. M. Veloso, H. F. M. Vester, A. Vicentini, I. C. G. Vieira, T. V. Bentos, G. B. Williamson, and D. M. A. Rozendaal
636 (2016). “Biomass resilience of Neotropical secondary forests”. *Nature* 530.7589, 211–214.



- 637 Poulter, B., L. Aragão, N. Andela, V. Bellassen, P. Ciais, T. Kato, X. Lin, B. Nachin, S. Luyssaert, N. Pederson, P.
638 Peylin, S. Piao, T. Pugh, S. Saatchi, D. Schepaschenko, M. Schelhaas, and A. Shivdenko (2019). The global forest age
639 dataset and its uncertainties (GFADv1.1). PANGAEA- Data Publisher for Earth & Environmental Science.
- 640 Pugh, T. A. M., M. Lindeskog, B. Smith, B. Poulter, A. Arneeth, V. Haverd, and L. Calle (2019). “Role of forest regrowth
641 in global carbon sink dynamics”. *Proceedings of the National Academy of Sciences* 116.10, 4382–4387.
- 642 Schepaschenko, D., A. Shvidenko, V. Usoltsev, P. Lakyda, Y. Luo, R. Vasylyshyn, I. Lakyda, Y. Myklush, L. See, I.
643 McCallum, S. Fritz, F. Kraxner, and M. Obersteiner (2017). “A dataset of forest biomass structure for Eurasia”.
644 *Scientific Data* 4, 170070.
- 645 Schimel, D. (2007). “Carbon cycle conundrums”. *Proceedings of the National Academy of Sciences* 104.47, 18353–
646 18354.
- 647 Somogyi, Z., M. Teobaldelli, S. Federici, G. Matteucci, V. Pagliari, G. Grassi, and G. Seufert (2008). “Allometric
648 biomass and carbon factors database”. *iForest - Biogeosciences and Forestry* 1.3, 107.
- 649 Sulla-Menashe, D., C. E. Woodcock, and M. A. Friedl (2018). “Canadian boreal forest greening and browning trends:
650 an analysis of biogeographic patterns and the relative roles of disturbance versus climate drivers”. *Environmental*
651 *Research Letters* 13.1, 014007.
- 652 Sullivan, M. J. P., J. Talbot, S. L. Lewis, O. L. Phillips, L. Qie, S. K. Begne, J. Chave, A. Cuni-Sanchez, W. Hubau, G.
653 Lopez-Gonzalez, L. Miles, A. Monteagudo-Mendoza, B. Sonké, et al. (2017). “Diversity and carbon storage across the
654 tropical forest biome”. *Scientific Reports* 7, 39102
- 655 Tramontana, G., M. Jung, C. R. Schwalm, K. Ichii, G. Camps-Valls, B. Ráduly, M. Reichstein, M. A. Arain, A. Cescatti,
656 G. Kiely, L. Merbold, P. Serrano-Ortiz, S. Sickert, S. Wolf, and D. Papale (2016). “Predicting carbon dioxide and
657 energy fluxes across global FLUXNET sites with regression algorithms”. *Biogeosciences* 13.14, 4291–4313.
- 658 Werf, G. R. v. d., J. T. Randerson, L. Giglio, T. T. v. Leeuwen, Y. Chen, B. M. Rogers, M. Mu, M. J. E. v. Marle, D. C.
659 Morton, G. J. Collatz, R. J. Yokelson, and P. S. Kasibhatla (2017). “Global fire emissions estimates during 1997–2016”.
660 *Earth System Science Data* 9.2, 697–720.
- 661 Williams, C. A., G. J. Collatz, J. Masek, and S. N. Goward (2012). “Carbon consequences of forest disturbance and
662 recovery across the conterminous United States”. *Global Biogeochemical Cycles* 26.1.
- 663 Woodbury, P. B., J. E. Smith, and L. S. Heath (2007). “Carbon sequestration in the U.S. forest sector from 1990 to
664 2010”. *Forest Ecology and Management*. 241: 14-27. 241.
- 665 Zhu, Z., S. Piao, R. B. Myneni, M. Huang, Z. Zeng, J. G. Canadell, P. Ciais, S. Sitch, P. Friedlingstein, A. Arneeth, C.
666 Cao, L. Cheng, E. Kato, C. Koven, Y. Li, X. Lian, Y. Liu, R. Liu, J. Mao, Y. Pan, S. Peng, J. Peñuelas, B. Poulter, T. A.
667 M. Pugh, B. D. Stocker, N. Viovy, X. Wang, Y. Wang, Z. Xiao, H. Yang, S. Zaehle, and N. Zeng (2016). “Greening of
668 the Earth and its drivers”. *Nature Climate Change* 6.8, 791–795.
- 669 Zscheischler, J., M. D. Mahecha, V. Avitabile, L. Calle, N. Carvalhais, P. Ciais, F. Gans, N. Gruber, J. Hartmann, M.
670 Herold, K. Ichii, M. Jung, P. Landschützer, G. G. Laruelle, R. Lauerwald, D. Papale, P. Peylin, B. Poulter, D. Ray, P.
671 Regnier, C. Rödenbeck, R. M. Roman-Cuesta, C. Schwalm, G. Tramontana, A. Tyukavina, R. Valentini, G. v. d. Werf, T.



- 672 O. West, J. E. Wolf, and M. Reichstein (2017). “Reviews and syntheses: An empirical spatiotemporal description of the
673 global surface–atmosphere carbon fluxes: opportunities and data limitations”. *Biogeosciences* 14.15, 3685–3703.
- 674 Zhang, Y., Y. Yao, X. Wang, Y. Liu, and S. Piao (2017). “Mapping spatial distribution of forest age in China”. *Earth and
675 Space Science* 4.3, 108–116.